

Experimental Study of Low-Pressure Automotive Cooling Fan Aerodynamics Under Blocked Conditions

Gifford N. L.*, Hunt A. G.*, Savory E.*, Martinuzzi R. J.**

*Dept of Mechanical and Materials Engineering, University of Western Ontario
London, Ontario, Canada (nlgiffor@uwo.ca , ahunt2@uwo.ca, esavory@eng.uwo.ca)

**Department of Mechanical and Manufacturing Engineering, University of Calgary
Calgary, Alberta, Canada (rmartinu@ucalgary.ca)

The present research examines the effect of a downstream-mounted blockage plate on the performance of low-pressure, axial-flow, automotive cooling fans (LPF). Measurements conducted in a plenum chamber quantify performance changes as a function of blockage distance. Three-component Laser Doppler Velocimetry (LDV) measurements were made of the downstream flow with and without blockage. Experiments were performed for two fan designs, one optimized for low flow rate, high-pressure operation, and a second optimized for high flow rate, low-pressure operation. The results show that the pressure loss caused by the blockage plate increases with increasing flow rate and decreasing blockage distance. LDV measurements show that the blockage plate causes a reduction in the flow rate, an increase in the reverse flow near the fan hub, and a dramatic increase in the radial flow. The relation between blockage to fan proximity and fan performance was established. It is found that the pressure change follows a quadratic function, but the coefficients are fan specific

1. INTRODUCTION

Front-end styling requirements in modern vehicles place greater emphasis on aesthetics and minimizing vehicle size than on providing adequate cooling. The design of modern vehicles highly restricts under-hood geometries, and places the engine block very close to the cooling fan. The outflow is, thus, in the radial direction. Since automotive cooling fans are axial flow machines, they operate outside of their design environment. In addition to the constrained engine bays, vehicles, especially Sports Utility Vehicles (SUVs) and light trucks, are increasingly operating at higher speeds while moving larger loads. This gives rise to the need for cooling fans that deliver high volumetric flow rates over a wide range of operating conditions. Low-Pressure Fans (LPF) meet such requirements by having relatively flat performance curves over a larger range of operating conditions than a High Pressure Fan (HPF). In order to develop a LPF that meets new and existing market requirements, a complete understanding of under-hood component effects on fan performance is required. Despite the

importance and practicality of this topic, hardly any work has been devoted to study blockage effects on fan performance. It is evident [1] that progress in automotive cooling systems requires a complete system approach with appropriate measurement techniques. The objective of the present research is to quantify, *experimentally*, the interaction between an axial flow fan and the engine compartment for development of a novel, highly optimized, low-pressure fan (LPF) design.

Various engine bay components are expected to affect fan performance. Those components are schematically shown in Figure 1. In order to simulate their effect, an *in-situ* test rig has been designed and constructed at The University of Western Ontario (UWO). The Laser Doppler Velocimetry (LDV) technique was chosen to gather detailed, non-intrusive, three-component velocity measurements in the fan wake. Use of a specially developed five-beam LDV probe was used to capture all three velocity components simultaneously. Using a conventional, two-probe setup was not practical in this highly constrained under-hood environment.

An additional set of experiments was conducted to demonstrate the relationship between fan performance and the distance from the fan to the engine blockage. These experiments were carried out in a plenum chamber located at Siemens VDO Automotive Inc., London, Ontario. Figure 2 shows an annotated photograph of a test fan and blockage plate installed in the plenum chamber.

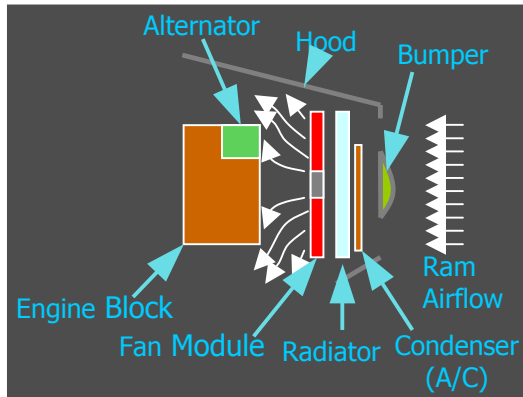


Figure 1: Engine Compartment Schematic

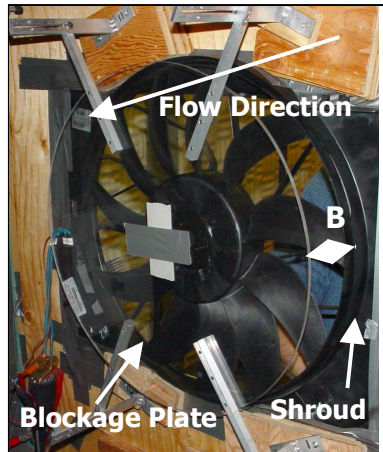


Figure 2: Fan mounted in the plenum chamber

2. BACKGROUND

Fan performance is usually measured in plenum chambers, where simulation of unobstructed, ideal fan performance is possible. Plenum chamber design is discussed in detail in AMCA standard 210-99 [2]. Equations 1-5 represent fan driving motor electrical power, output air power, module efficiency, rotor static fan efficiency and torque, respectively. Output air power is calculated on a control volume surrounding the fan as defined by AMCA [2] and assumes steady state flow and constant density.

$$\hat{P}_{in} = VI \quad (1)$$

$$\hat{P}_{out} = P_s \cdot \dot{Q} \quad (2)$$

$$\eta = \frac{\hat{P}_{out}}{\hat{P}_{in}} = \frac{P_s \cdot \dot{Q}}{V \cdot I} \quad (3)$$

$$\eta_{fan} = \frac{\eta}{\eta_{motor}} \quad (4)$$

$$T = \frac{\hat{P}_{out}}{\omega} = F \cdot r \quad (5)$$

To facilitate comparison with different sized fans, non-dimensional groupings are used, as in other turbomachinery design. Equations 6-8 represent the flow, pressure and power coefficients. Equation 9 is the Reynolds number based on fan diameter and equation 10 is a non-dimensional representation of blockage distance that is used in the present paper to develop a generalized equation of blockage distance effects on fan performance.

$$\phi = \frac{\dot{Q}}{\omega \cdot D^3} \quad (6)$$

$$\psi = \frac{P_s}{\rho \omega^2 D^2} \quad (7)$$

$$\hat{P}^* = \frac{\hat{P}}{\rho \omega^3 D^5} \quad (8)$$

$$Re_D = \frac{\rho \omega D^2}{\mu} \quad (9)$$

$$\Delta = B/D \quad (10)$$

LDV has been used in various published studies to measure fan aerodynamics. Jang et al. [3] used LDV to measure the flow downstream of a propeller fan, and compared their results with Large Eddy Simulation (LES) results. They found a large vortex that travels through the tip gap, which was predicted remarkably well in terms of size and position by the LES simulation despite having simplified the geometry to an axisymmetric one. This suggests that the current implementation of a generic *in-situ* facility will still provide a model that accurately simulates vehicle engine bay aerodynamics.

In a blocked environment, it is postulated that radial flow will be more pronounced due to the

turning of the flow around the blockage. Vad and Bencze [4] used LDV to quantify the radial velocity profiles of several fans. Their conclusion is that radial velocity is important to fan performance and that the efficiency and pressure rise can be improved through consideration of radial velocity in the design process.

Morris et al. [5] used hot-wire anemometry (HWA) to measure the flow field of an isolated axial flow fan. The high sampling rates of HWA allowed data to be sampled for every degree of rotation. By sampling 900 fan revolutions over 30s, Morris was able to sample 900 data points in each phase-averaged bin. He found areas of flow recirculation in the hub region and behind the blades, which is indicative of stall inception. Also, high positive, fluctuating and unsteady radial flows were found along with strong tangential velocities up to 40% of the tip speed. The recommendation of the work was to implement non-intrusive LDV measurements to survey velocity data in the inter-blade region.

The present research aims to build upon these prior studies by quantifying the aerodynamics of an automotive cooling fan within its operating environment, namely the engine compartment. With a detailed understanding of the realistic fan boundary conditions found *in-situ*, a fully optimized fan design will be realizable.

3. EXPERIMENTAL SETUP

Two fans were tested in detail for both experiments. While one fan exhibits low-pressure characteristics, the other represents a more typical fan curve. Table 1 lists the relevant operational and design parameters of each test fan. LDV tests were conducted at the vehicle 'idle' condition, which corresponds to a zero forward velocity. When a vehicle is at rest, the fan flow rate is fixed by the sum of pressure losses induced by the *in-situ* facility, radiator and a downstream engine blockage. Provision of ram air was not included in the scope of the experimentation. Each fan was tested at its respective maximum speed both with and without a 520mm disc positioned in the wake of the fan to simulate the engine blockage. The diameter of the disc was chosen to be equivalent to the outer fan shroud diameter.

To determine the effect of blockage distance on overall fan performance, a series of experiments

were conducted in the plenum chamber. For the two test fans, the blockage distance, as measured from the blade trailing edge, was varied from 55mm to 105mm. A full set of fan performance characteristics were then measured from the zero flow rate condition, where the fan is most highly loaded, to the condition of least blade loading where the outlet pressure equals atmospheric pressure. Figure 3 depicts example fan performance curves for the conventional type and LPF type fans, along with the total system resistance for different vehicle speeds. The fan operating point is determined by the intersection of the fan performance and system resistance curves. The difference in each curve as compared to an unblocked test is then calculated and plotted. The quadratic regression coefficients for the pressure difference are then plotted as a function of non-dimensional blockage distance. The resulting plots give the coefficients of pressure loss as a function of blockage distance and fan diameter.

A second experiment involved detailed flow measurements downstream of the fan using LDV. The LDV probe is located beside the *in-situ* facility so as not to intrude into the flow. A 750mm focal length lens and a 2.6X beam expander are used to focus the measurement volume downstream of the fan. To seed the flow, atomized olive oil was injected upstream of the radiator such that a stream of particles passed through the measurement volume. The particles were measured using Phase Doppler Anemometry to have a mean diameter of approximately 1 μ m with 90% of particles smaller than 2 μ m. This technique enabled data rates of up to 1000Hz in coincident measurement mode. For all measurements, a coincident window setting of 400 μ s was used. The coincidence window was selected to be at a point where the cross-correlation coefficient is independent of coincidence window length. The LDV measurement volume is 2.7, 1.3, and 2.5mm in length and it is 115, 110 and 108 μ m in diameter for the green, blue and violet beams, respectively. Measurement volume positioning is accomplished with a three-axis Cartesian traverse with a spatial accuracy of 0.1mm.

At each measurement location, 50,000 points of velocity data were collected. This corresponds to a measurement time of 50-100s and between 2000 and 4000 fan rotations. Measurements were taken 3mm (approximately 5% of chord) downstream of the blade trailing edge and every

15mm radially, to determine how blockage affects the flow leaving the fan blades. Measurements of flow this close to the blade are assumed by the authors to be equivalent to the flow leaving the fan blade trailing edge. The amount of data recorded enables accurate mean velocity calculations of the phase-averaged data. Transit time weighting is applied to all velocity measurements. The data are then phase averaged into three-degree-wide bins using Matlab, resulting in a minimum of 300 data points per bin. To phase average, each rotational period must be individually determined by comparing the number of data points in the first and last time-bins. When these are within 80% of each other, the rotational period is accurate to within one bin width, or approximately 0.25ms. All data are then divided into bins according to the rotational period. As an additional check, a maximum of 1% of data could be excluded if they lay outside of the average rotational period.

The location of the measurements in relation to the fan shroud corresponds to the 180-degree line in Figure 4. This location was chosen, as it is the only area with sufficient optical access to measure within 3mm of the blade trailing edge across the entire blade span.

Table 1 – Fan Operational and Design Parameters

Characteristic	Low-Pressure Fan	Conventional Fan
Tip Diameter	487mm	487mm
Number of Blades	7	8
Sweep Direction	Backward	Backward
Operating Speed	2400 rpm	2100 rpm
Power Consumption	600W	400W
Airfoil Profile	DLR-2	DLR-2
<i>LDV Test Conditions</i>		
Flow Rate	1.136 m ³ /s	0.864 m ³ /s
Static Pressure	49.4 Pa	123 Pa
<i>Blade Parameters (calculated at mid-span)</i>		
Chord Length	56mm	63mm
Stagger Angle	71.4°	76.4°

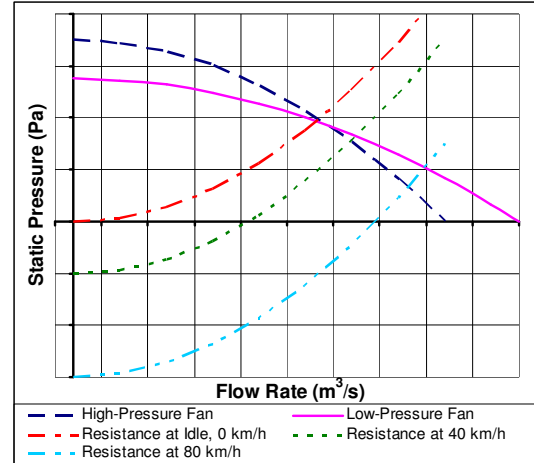


Figure 3: Example Fan Performance and System Resistance Curves



Figure 4: Measurement Plane

4. DATA ANALYSIS

In this analysis, fan performance data as it relates to blockage distance is first presented and discussed. This is followed by an analysis of the aerodynamic measurement results.

4.1 BLOCKAGE EFFECTS ON FAN PERFORMANCE

Fan performance curves were generated to illustrate the effect of a blockage plate on overall fan performance characteristics. Figure 5 shows the fan pressure as a function of flow rate for the HPF while Figure 6 shows the same for the LPF. The measurements are accurate to within 2% in pressure and flow rate according to the AMCA standard [2]. It is clear for the HPF that fan throughput decreases as the blockage plate distance (B) is reduced. For the LPF, however, the loss in pressure output with blockage is much less pronounced than for the HPF design. This is due to the LPF being closer to its design

operating point at high flow rates.

A correlation between blockage distance and the pressure loss induced by a blockage plate is sought to aid in determining realistic boundary conditions. First, the difference in pressure between each blocked performance curve and the unblocked one is calculated. This difference is then fit to a quadratic equation and the coefficients of the equations for each blockage distance are plotted versus inverse non-dimensional blockage distance (Δ) (Figures 7 and 8). From this plot, a quadratic equation for pressure loss coefficient as a function of blockage distance and flow coefficient of the form $\delta\psi = i\phi^2 + j\phi + k$ can be determined. See equation 11 for the HPF and 12 for the LPF.

$$\delta\psi = (-0.05405\Delta^{-3} + 0.5277\Delta^{-2} - 1.408\Delta^{-1})\phi^2 + (0.003545\Delta^{-3} - 0.03907\Delta^{-2} + 0.07835\Delta^{-1})\phi + 0 \quad (11)$$

$$\delta\psi = (-0.05905\Delta^{-3} + 0.3594\Delta^{-2} - 1.082\Delta^{-1})\phi^2 + (0.004577\Delta^{-3} - 0.02994\Delta^{-2} + 0.07229\Delta^{-1})\phi + 0 \quad (12)$$

Equations 11 and 12 are shown to collapse the blocked performance in Figure 9 and 10 where $\delta\psi_{\text{measured}} - \delta\psi_{\text{predicted}}$ is plotted. The HPF plot shows that the pressure difference is slightly over-predicted at low blockage distances and under-predicted at large distances. For the LPF, the results are better, not showing any consistent estimation errors.

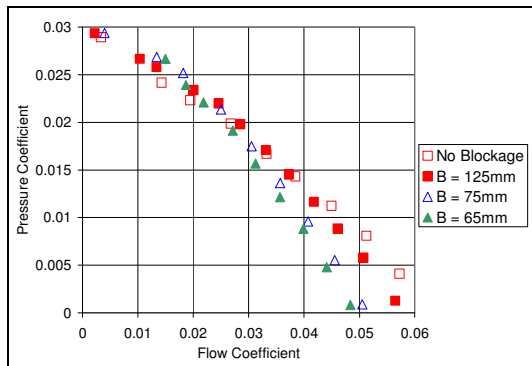


Figure 5: Conventional Fan Performance with Varying Blockage Distance

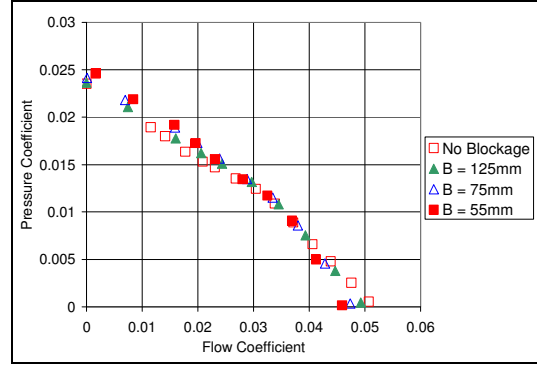


Figure 6: LPF Performance with Varying Blockage Distance

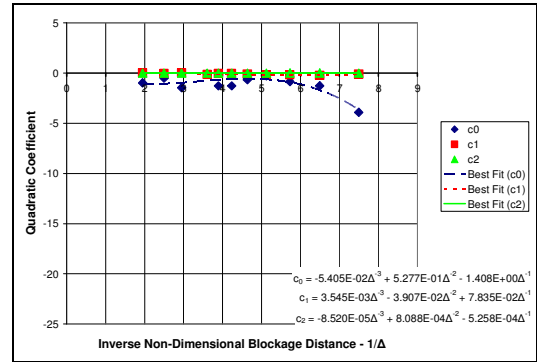


Figure 7: Pressure Loss Coefficients Plotted Against $1/\Delta$ (HPF)

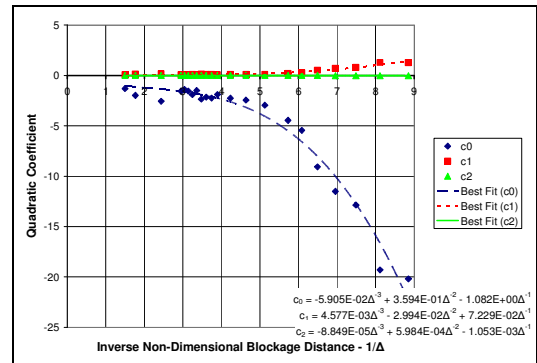


Figure 8: Pressure Loss Coefficients Plotted Against $1/\Delta$ (LPF)

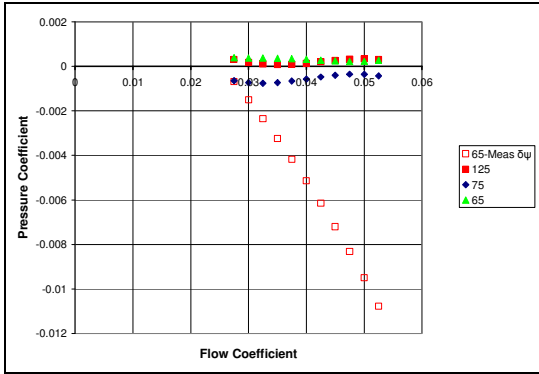


Figure 9: Collapse of $\delta\psi$ using Eq 11 (HPF) Compared to Measured $\delta\psi$

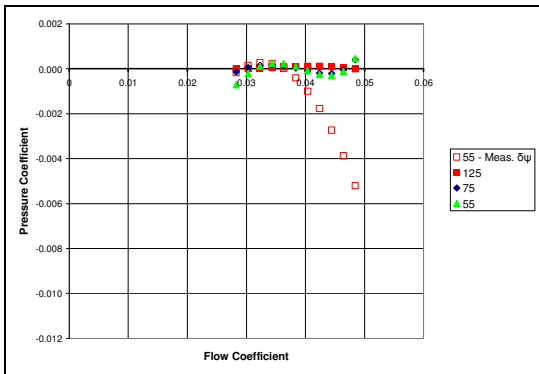


Figure 10: Collapse of $\delta\psi$ using Eq 12 (LPF) Compared to Measured $\delta\psi$

4.2 DOWNSTREAM FLOW MEASUREMENTS

LDV measurements conducted 3mm downstream of the blade trailing edge were phase-averaged into 120 three-degree-wide bins. Vector plots of the mean, phase-averaged radial and tangential velocities projected in the axial plane and coloured by axial velocity (C_x) are shown in Figures 11 – 14. The arrowhead size is proportional to the vector length for enhanced visibility. A plot of the time-averaged mean radial velocity is presented in Figure 15.

Figures 11 and 12 show the effect of blockage on the low-pressure fan. The blockage plate causes a reduction in flow rate due to the increase in back pressure, which in-turn reduces the axial velocities, especially near the tips. There is also a much larger stagnant flow region near the hub, with greater reversed flow under blockage. Most importantly, the blockage plate causes increased radial flow at the blade trailing edge. It can be deduced that the increased radial flow increases the effective blade chord because the flow has

further to travel over the blade surface. Thus, the effective camber will be reduced by a similar factor since the deflection of the flow in the tangential direction remains constant.

Absolute velocity vectors for the unblocked and blocked conventional fan are shown in Figures 13 and 14. Again, the trend is towards lower flow rate and axial velocity, and increased reversed flow near the hub region. The radial flow is also increased, but not to the same extent as for the low-pressure fan.

By comparing the analysis of Figures 11 and 12 for the low-pressure fan, and Figures 13 and 14 for a conventional fan, it is possible to assess how each type of fan interacts with a blockage. The main difference is that the low-pressure fan exhibits a much greater increase in radial flow under blockage. To examine this in more detail, time-averaged mean radial flow is plotted in Figure 15 for each test case. For the unblocked cases, the radial outflow is largely due to the action of the flow moving over the hub. However, in the blocked cases, the radial flow is induced by the action of the flow moving around the blockage plate. The low-pressure fan likely exhibits a more marked increase in radial flow because this fan is more highly loaded, and is therefore nearer to a radial flow regime than the conventional design. Eck [6] found that flow vectors are axial at the design flow rate, and gradually become radial as flow rate decreases. This is due to the formation of a vortex at the hub that deflects flow radially. As the flow rate decreases, a second vortex forms at the tip and causes radial flow across the entire blade span.

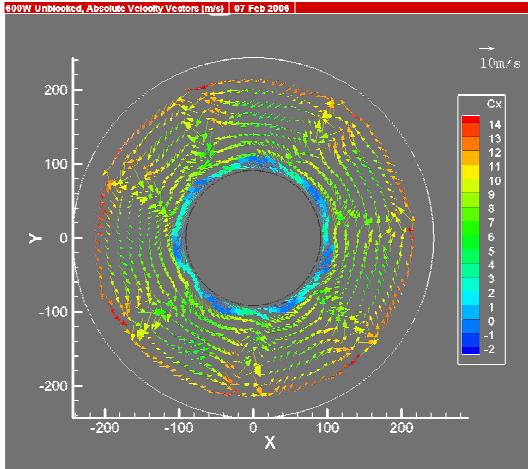


Figure 11: Absolute Velocity Vectors: Unblocked Low-Pressure Fan

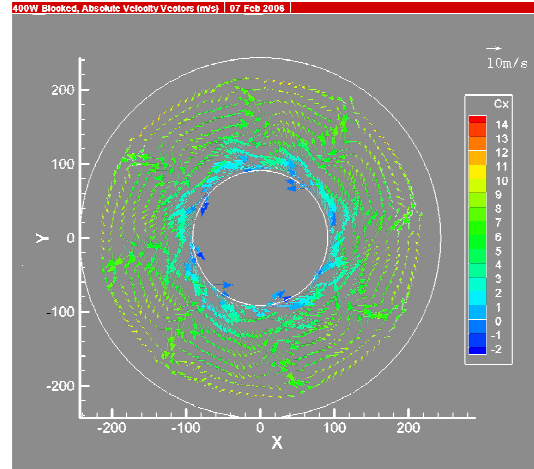


Figure 14: Absolute Velocity Vectors: Blocked Conventional Fan

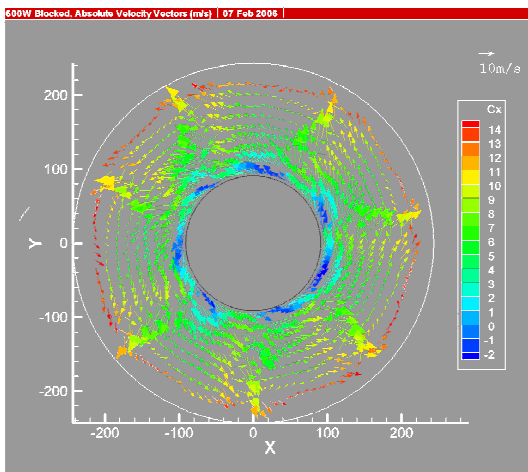


Figure 12: Absolute Velocity Vectors: Blocked Low-Pressure Fan

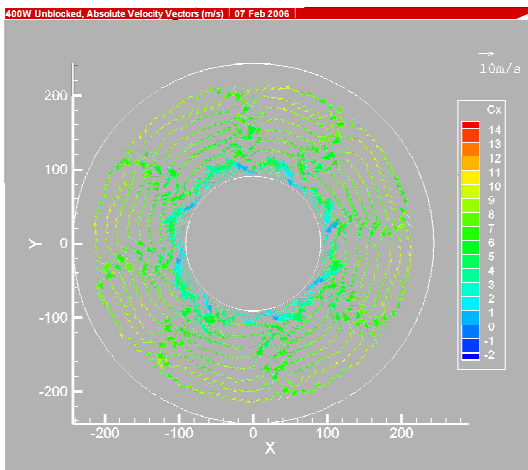


Figure 13: Absolute Velocity Vectors: Unblocked Conventional Fan

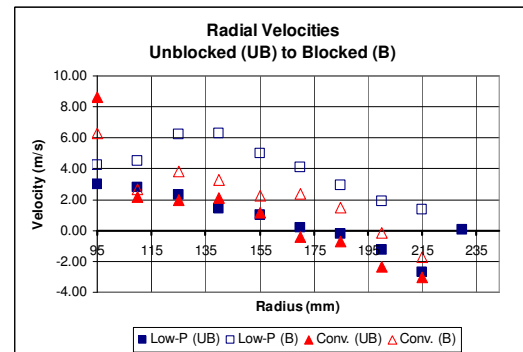


Figure 15: Mean Radial Velocity Comparison (Conv.=conventional fan, Low-P=low-pressure fan)

5. CONCLUSIONS

Measurements were conducted to demonstrate the aerodynamic and performance implications of downstream blockages on automotive axial-flow cooling fans. The results have demonstrated that the blockage plate causes a pressure loss in the system that increases with flow rate and decreasing blockage distance. The LPF exhibits less blockage-induced pressure loss at high flow rates than the conventional fan due to its design operating point being at a higher flow rate. Equations to relate pressure loss to non-dimensional blockage distance (Δ) successfully collapse the data onto the no-blockage case. These equations can be used to predict fan performance under blockage and to determine at what distance (B) the blockage pressure loss becomes significant. More work is required to develop a single relation which works for different fan types, however.

A second set of non-intrusive velocity measurements show the effect of a blockage plate at the exit plane of the fan. From these results, it can be concluded that the blockage plate reduces overall flow rate, increases reversed flow near the hub and increases the radial flow across the blade span. The literature suggests that fan performance and efficiency can be improved by accounting for radial flow in the design process. Lastly, the LPF design exhibits greater radial flow under blockage. The LPF is designed for high flow rate operation. However, the LDV measurements are conducted at low flow rates, and therefore it is operating farther from its design point than the HPF. This could account for the increased radial flow according to Eck [6].

6. ACKNOWLEDGEMENTS

The authors are grateful for the financial support of both Siemens VDO Automotive and Materials and Manufacturing Ontario under Research Project No. DE40094. We would also like to thank Ms. Rita Patel and Mr. James Kempston for their help taking and processing measurements. We would also like to thank Brian Havel (Siemens VDO) for his guidance and advice as well as Ehab Abu Ramadan (UWO) for graciously reviewing this paper.

7. REFERENCES

- [1] Ng E.Y., Watkins S., Johnson P.W., and Mole L. Measuring local time-averaged airflow *Proc 14th Australian Fluid Mechanics Conf.*, Adelaide, Australia, 2001.
- [2] AMCA Standard 210-99: Laboratory Methods of Testing Fans for Aerodynamic Performance Rating, AMCA, 1999.
- [3] Jang C.M., Furukawa, M. and Inoue, M. Analysis of the vortical flow field in a propeller fan by LDV measurements and LES, *Transactions of the ASME*, **123**:748-761, 2001.
- [4] Vad, J. and Bencze, F. Three-dimensional flow in axial flow fans of non-free vortex design, *International Journal of Heat and Fluid Flow*, **19**:601-607, 1998.
- [5] Morris S.C., Good, J.J. and Foss, J.F. Velocity measurements in the wake of an

automotive cooling fan, *Experimental Thermal and Fluid Science*, **17**:100-106, 1998.

- [6] Eck, B. Fans: design and operation of centrifugal, axial-flow, and cross-flow fans, Pergamon Press, New York, 1973.

NOMENCLATURE

- B blockage distance [m]
 c_y tangential velocity [m/s]
 c_r radial velocity [m/s]
 c_x axial velocity [m/s]
D fan diameter [m]
F force exerted by fluid on fan blade [N]
I current input to the driving motor [A]
 \hat{P} non-dimensional fan power
 \hat{P}_{in} power input to the fan motor [W]
 \hat{P}_{out} power output to the working fluid [W]
 P_s static pressure rise across the fan rotor [Pa]
 \dot{Q} flow rate through the fan [m³/s]
r fan radius [m]
 Re_D Reynolds number based on fan diameter
T torque output from the driving motor [Nm]
V voltage input to the driving motor [V]
 η fan efficiency
 Δ non-dimensional blockage distance
 ϕ flow coefficient
 ρ fluid density [kg/m³]
 ω rotational speed [rad/s]
 ψ pressure coefficient